Phytochemistry 184 (2021) 112656

Contents lists available at ScienceDirect

Phytochemistry

journal homepage: www.elsevier.com/locate/phytochem

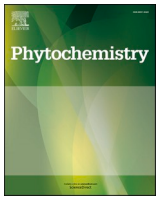

Previously undescribed pyridyl-steroidal glycoalkaloids and 23*S*,26*R*-hydroxylated spirostanoid saponin from the fruits of *Solanum violaceum* ortega and their bioactivities

Joseph Sakah Kaunda [a,b], Xu-Jie Qin [a,c], Hong-Tao Zhu [a,c], Dong Wang [a,c], Chong-Ren Yang [a], Ying-Jun Zhang [a,c,*]

[a] State Key Laboratory of Phytochemistry and Plant Resources in West China, Kunming Institute of Botany, Chinese Academy of Sciences, Kunming, 650204, PR China
[b] University of Chinese Academy of Sciences, Beijing, 100049, PR China
[c] Yunnan Key Laboratory of Natural Medicinal Chemistry, Kunming Institute of Botany, Chinese Academy of Sciences, Kunming, 650204, PR China

ARTICLE INFO

Keywords:
Solanum violaceum
Solanaceae
Glycoalkaloids
Solanindiosides A-C
23S,26R-hydroxylated spirostanoid saponin
Lignans
Cytotoxicity
Apoptosis
Antibacterial
Staphylococcus aureus

ABSTRACT

Three previously undescribed pyridyl-steroidal glycoalkaloids, solanindiosides A–C, one rare 23*S*,26*R*-hydroxylated spirostanoid saponin, and two steroidal alkaloid aglycones, solanindins A and B, derived from the acid hydrolysis of solanindiosides A–C, were isolated from the fruits of *Solanum violaceum*, together with five known analogues, including two rare steroidal glycosides, two lignans and a diterpene. Structurally, they comprise a 16β-methoxy-23-deoxy-22,26-epimino-cholest-type skeleton moiety, and a 16β-methoxy-3,23-dideoxy-22,26-epimino-cholest-3,5-dien derivative. The hitherto undescribed structures were established on the basis of extensive spectroscopic analyses. Configurations of sugar moieties were resolved by chemical derivations. Solanindiosides A–C, (22*R*,23*S*,25*R*,26*R*)-spirost-5-ene-3β,23,26-triol3-*O*-β-D-xylopyranosyl-(1→3)-β-D-glucopyranoside, solanindins A and B, and (1*S*,2*S*)-1-(4-hydroxy-3-methoxyphenyl)-2-[2-methoxy-4-[(2*S*,3*R*,4*R*)-tetrahydro-4-[(4-hydroxy-3-methoxyphenyl)methyl]-3-(hydroxymethyl)-2-furanyl]phenoxy]-1,3-propanediol were evaluated for their cytotoxic and antibacterial activities. (1*S*,2*S*)-1-(4-hydroxy-3-methoxyphenyl)-2-[2-methoxy-4-[(2*S*,3*R*,4*R*)-tetrahydro-4-[(4-hydroxy-3-methoxyphenyl)methyl]-3-(hydroxymethyl)-2-furanyl]phenoxy]-1,3-propanediol showed the most potent cytotoxic activity against MCF-7 cells (IC_{50} = 4.386 ± 0.098 μM), while solanindin B displayed some inhibitory effects against *Staphylococcus aureus* Rosenbach with MIC_{50} value of 37.32 ± 0.793 μM. In addition, (1*S*,2*S*)-1-(4-hydroxy-3-methoxyphenyl)-2-[2-methoxy-4-[(2*S*,3*R*,4*R*)-tetrahydro-4-[(4-hydroxy-3-methoxyphenyl)methyl]-3-(hydroxymethyl)-2-furanyl]phenoxy]-1,3-propanediol induced dose dependent apoptosis effect in MCF-7 cells.

1. Introduction

Plants synthesizing nitrogen containing alkaloids have been demonstrated to be of great pharmaceutical interest. Research has evidenced that members of the families Solanaceae, Apocynaceae, Liliaceae and Buxaceae are a bountiful source of these alkaloids (Augustin et al., 2015). The genus *Solanum*, with about 1500 species distributed across Americas, Australia, Africa and Asia, offers medicinal, economic, and ornamental benefits (Kaunda and Zhang, 2019a; Yahara et al., 1996). Phytochemical studies on *Solanum* species have demonstrated their repository of steroidal alkaloids, steroidal saponins, flavonoids, terpenes, lignans, phenolics, sterols and coumarins (Kaunda and Zhang, 2019a, 2020). Some among them possess antibacterial, anticancer, antidiabetic, anti-inflammatory and hepato-protective properties (Kaunda and Zhang, 2019a).

Solanum violaceum Ortega (Solanaceae, synonym *Solanum indicum* var. *recurvatum* C.Y. Wu & S.C. Huang) is distributed mainly in China, India, Jawa, Laos, Bangladesh, East Himalaya, Hainan, Myanmar, Pakistan, Yemen, Vietnam, Philippines, Assam, Saudi Arabia, Sri Lanka, Taiwan, and Thailand (Kaunda and Zhang, 2020; http://www.plants of the world online. org/taxon/urn:lsid:ipni.org:names:821485-1). Our previous investigation on its fruit methanolic extract revealed four

* Corresponding author. State Key Laboratory of Phytochemistry and Plant Resources in West China, Kunming Institute of Botany, Chinese Academy of Sciences, Kunming, 650204, PR China.
E-mail address: zhangyj@mail.kib.ac.cn (Y.-J. Zhang).

https://doi.org/10.1016/j.phytochem.2021.112656
Received 29 October 2020; Received in revised form 31 December 2020; Accepted 3 January 2021
Available online 29 January 2021

steroidal saponins, one steroidal sapogenin and two ketosteroids (Kaunda and Zhang, 2020). Further studies on the above extract uncovered previously undescribed pyridyl-type steroidal glycoalkaloids (**1**–**3**), 23*S*,26*R*-hydroxylated spirostanoid saponin (**4**), two aglycones (**5**–**6**), alongside five known constituents (**5**–**9**). Compounds **1**–**6** and **9** were evaluated for their cytotoxic and antibacterial activities. Furthermore, **9** was evaluated for its apoptosis effect in MCF-**7** cells. Herein, we report the study.

2. Results and discussion

2.1. Isolation and structure elucidation

The MeOH extract of the air-dried fruits of *S. violaceum* was partitioned between *n*-butanol and water. The *n*-butanol extract was then subjected to repeated column chromatography (CC), leading to the isolation of three previously undescribed pyridyl-type steroidal glycoalkaloids (**1**–**3**), one steroidal saponin (**4**), and two aglycones (**5**–**6**) by acidic hydrolysis of **1**–**3** (Fig. 1), together with five known compounds identified as two rare steroidal glycosides, indiosides A (**7**) (Mona et al., 2009) and F (**8**) (Mona et al., 2009; Nafady et al., 2003), two lignans, (1*S*,2*S*)-1-(4-hydroxy-3-methoxyphenyl)-2-[2-methoxy-4-[(2*S*,3*R*, 4*R*)-tetrahydro-4-[(4-hydroxy-3-methoxyphenyl)methyl]-3-(hydroxymethyl)-2-furanyl] phenoxy]-1,3-propanediol (**9**) (Cutillo et al., 2003), lariciresinol dimethyl ether (**10**) (Ayoub et al., 1984), and a diterpene, ent-16α,17-dihydroxyatisan-3-one (**11**) (Satti et al., 1987) (Fig. S1, Supplementary data).

Solanindioside A (**1**) was isolated as a white amorphous powder, positive to Dragendorff test, and gave a molecular formula of $C_{45}H_{67}NO_{16}$, owing to a molecular ion peak at *m/z* 878.4536 $[M + H]^+$ (calcd for $C_{45}H_{68}NO_{16}$, 878.4533), in the HRESIMS. The IR spectrum of **1** displayed absorption bands for hydroxy (3424 cm^{-1}), carboxylic acid (2934 cm^{-1}), C═N (1632 cm^{-1}), C–O (1044 cm^{-1}) functionalities. The ^{1}H NMR spectrum of **1** (Table 1) showed two tertiary methyls at δ_H 0.56 and 1.02 (each 3H, s, CH_3-18, CH_3-19), two secondary methyls at δ_H 1.46 (3H, d, $J = 7.2$ Hz, CH_3-21) and δ_H 2.31 (3H, s, CH_3-27), which are characteristic signals of a steroidal compound (Kasai et al., 1979), three olefinic

Signals at δ_H 5.39 (1H, br. d, $J = 5.0$ Hz, H-6), 7.51 (1H, s, H-24), 7.11 (1H, s, H-26), one methoxyl at δ_H 3.18, and three anomeric signals at δ_H 4.51 (1H, d, $J = 7.8$ Hz), 5.23 (1H, s), 4.39 (1H, d, $J = 7.7$ Hz), suggesting that **1** constituted of three sugar moieties. The ^{13}C NMR and DEPT spectra of **1** (Table 1) showed a total of 45 signals; 28 signals, including an oxygenated methane, three tri-substituted double bonds, seven methylenes, five methines, four methyl groups, one methoxy group, and seven quaternary carbons, were assigned to the aglycone of the glycoside, and 17 signals were ascribable to two hexosyl and one pentosyl sugar moieties which, based on *J* values (Kasai et al., 1979; Ripperger, 1996) and acidic hydrolysis, followed by GC analysis of the corresponding trimethylsilylated L-cysteine adduct, were determined to be β-D-glucosyl, α-L-rhamnosyl and β-D-xylosyl units, respectively. In the HMBC experiment, correlations from H_3-18 (δ_H 0.56) to C-13 (δ_C 44.9), C-14 (δ_C 55.5), C-12 (δ_C 39.6) and C-17 (δ_C 62.6), from H_3-19 (δ_H 1.02) to C-5 (δ_C 142.1), C-9 (δ_C 51.3), and C-10 (δ_C 38.0), from H_3-21 (δ_H 1.46) to C-17 (δ_C 62.6), C-20 (δ_C 36.0) and C-22 (δ_C 151.0), from H_3-27 (δ_H 2.31) to C-24 (δ_C 120.3), C-25 (δ_C 139.6), and C-26 (δ_C 134.7), from H-24 (δ_H 7.51) to C-22 (δ_C 151.0), C-25 (δ_C 139.6), C-26 (δ_C 134.7), and C-27 (δ_C 18.2), from H-26 (δ_H 7.11) to C-22, C-24, C-27, from H-17 (δ_H 2.19), H-20 (δ_H 3.56), and H_3-21 (δ_H 1.46) to C-22, and from H_2-15, H-17, H-20, and a methoxy group (δ_H 3.18) to C-16 (δ_C 116.2), alluded to the presence of a 16-methoxy-23-deoxy-22,26-epimino-cholest-type moiety (Xu et al., 2018) (Fig. 2), and instructed the assembling of A–F rings. Moreover, the UV spectra (λ_{max} 330, 260 nm), suggested the presence of a pyridine moiety, even as indicated by the two broad proton singlets at δ_H 7.51 (H-24) and δ_H 7.11 (H-26), and a proton singlet for an aromatic methyl group at δ_H 2.31 (H_3-27) (Abdel-Kader et al., 2000). On the pyridine ring, the location of the methyl group was further confirmed by ROESY correlations observed between δ_H 2.31 (H_3-27) and δ_H 7.51 (H-24)/7.11 (H-26). The HMBC correlations, from the rhamnosyl H-1" (δ_H 5.23) to glucosyl C-2' (δ 78.6), and the xylosyl H-1‴ (δ_H 4.39) to glucosyl C-3' (δ_C 88.2). Consequently, these correlations steered the assignment of the glycosidic moiety as α-L-rhamnopyranosyl-(1→2)-*O*-[β-D-xylopyranosyl-(1→3)]-β-D-glucopyranoside. The HMBC observed from the glucosyl H-1' (δ_H 4.51) to the aglycone C-3 (δ_C 78.8), ensured the connection of the sugar moiety to the aglycone C-3 through an *O*-linkage, as shown in Fig. 2. A thorough cross reference of 1D NMR data of the aglycone of **1** revealed that it possessed the same A-F rings as those of 16,23-epoxy-22,26-epimino-cholest-22(*N*),23,25 (26)-trien-3-
β-ol-3-*O*-β-D-glucopyranosyl-(1→2)-β-D-glucopyranosyl-(1→4)-β-D-galactopyranoside, a known steroidal alkaloid from *Solanum lyratum* Thunb. (Xu et al., 2018). However, the ^{13}C NMR resonance due to the C-16 of E ring of **1** was different from that of the above mentioned known compound. The C-16, an oxymethine, of the known compound was assigned δ_C 76.6 (Xu et al., 2018). In contrast, the C-16 of **1** was assigned δ_C 116.2, and this lower-field shifted value was commensurate with the proposed *O*-linkage between C-16 and C-23 in **1**, and the presence of OMe on C-16. The relative configurations of the aglycone of **1** were determined by the ROESY correlations of Me-19/H-2b, H-4b/H-8, H-3/H-2a, Me-19/H-11b, and H-11a/H-9/H-14, which indicated the α-orientation of H-3, H-9, H-14, and β-orientation of H-8; the ROESY correlation of Me-18 with H-20 suggested the α-orientation for Me-21 and β-orientation for H-20 (Fig. 3) (Li et al., 2016). The signal, H_3-18 (δ_H 0.56) of **1** was significantly

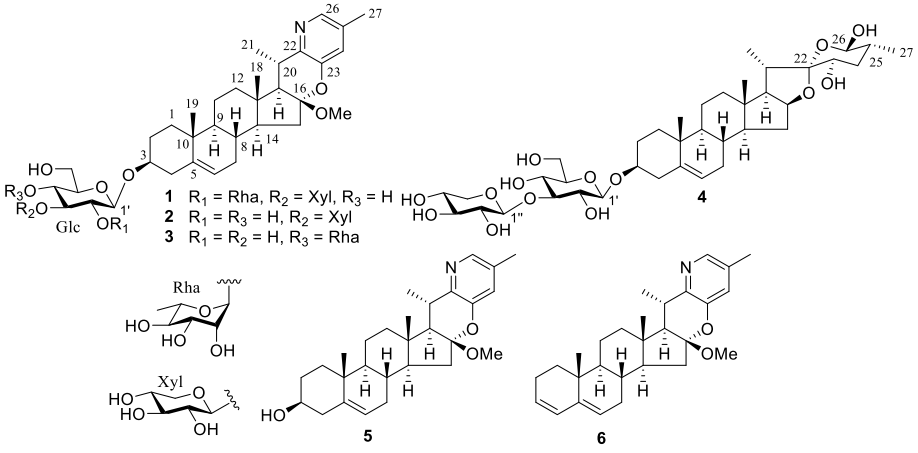

Fig. 1. Chemical structures of compounds 1–6.

Table 1
^{13}C and ^{1}H NMR data for **1–3** in CD_3OD (δ in ppm)[a].

No.	1		2		3	
	δ_C	δ_H (J in Hz)	δ_C	δ_H (J in Hz)	δ_C	δ_H (J in Hz)
1	38.4 t	1.90[b]; 1.11, m	38.4 t	1.89[b]; 1.11, m	38.4 t	1.88[b]; 1.10, m
2	30.7 t	1.90[b]; 1.61, m	30.6 t	1.94, m; 1.62, m	30.7 t	1.93, m; 1.61, m
3	78.8 d	3.64[b]	79.7 d	3.60, m	79.8 d	3.56, m
4	39.6 t	2.47, m; 1.88, m	39.6 t	2.44[b]; 1.88, m	39.7 t	2.44[b]; 1.88[b]
5	142.1 s		142.1 s		142.2 s	
6	122.2 d	5.39, d (5.0)	122.1 d	5.39, d (5.1)	122.1 d	5.38, d (5.0)
7	33.0 t	2.05, m; 1.65, m	33.0 t	1.66, m; 2.05, m	33.0 t	2.05, m; 1.65, m
8	32.3 d	1.63, m	32.3 d	1.64, m	32.3 d	1.63, m
9	51.3 d	1.06, m	51.3 d	1.08, m	51.3 d	1.08, m
10	38.0 s		38.0 s		38.0 s	
11	21.5 t	1.63, m; 1.50, m	21.5 t	1.64, m; 1.52, m	21.5 t	1.63, m; 1.51, m
12	39.6 t	2.47, m; 1.88[b]	39.6 t	2.44[b]; 1.89,[b]	39.6 t	2.44[b]; 1.89, d (4.2)
13	44.9 s		44.9 s		44.9 s	
14	55.5 d	1.52, m	55.5 d	1.52, m	55.5 d	1.52, m
15	40.5 t	2.53, dd (13.0, 5.9) 1.88[b]	40.5 t	2.53, dd (13.0, 5.9) 1.89[b]	40.5 t	2.54, dd (13.0, 5.9) 1.88[b]
16	116.2 s		116.2 s		116.2 s	
17	62.59 d	2.19, s	62.59 d	2.20, s	62.6 d	2.19, s
18	14.1 q	0.56, s	14.1 q	0.56, s	14.1 q	0.56, s
19	19.8 q	1.02, s	19.8 q	1.03, s	19.8 q	1.02, s
20	36.0 d	3.56, q (7.4)	36.0 d	3.57, q (6.5)	36.0 d	3.58, m
21	18.2 q	1.46, d (7.2)	18.2 q	1.47, d (7.3)	18.2 q	1.47, d (7.3)
22	151.0 s		151.0 s		151.0 s	
23	165.1 s		165.1 s		165.1 s	
24	120.3 d	7.51, s	120.3 d	7.51, s	120.3 d	7.51, s
25	139.6 s		139.6 s		139.6 s	
26	134.7 d	7.11, s	134.7 d	7.11, s	134.7 d	7.11, s
27	18.2 q	2.31, s	18.3 q	2.31, s	18.3 q	2.31, s
OMe	52.5 q	3.18, s	52.5 q	3.18, s	52.5 q	3.18, s
	3-*O*-Glc		3-*O*-Glc		3-*O*-Glc	
1′	100.3 d	4.51, d (7.8)	102.1 d	4.43, d (7.9)	102.4 d	4.39, d (7.9)
2′	78.6 d	3.47, m	74.4 d	3.32, m	75.2 d	3.18, s
3′	88.2 d	3.64[b]	87.9 d	3.48, m	76.7 d	3.45, m
4′	69.88 d	3.33, m	69.9 d	3.34, m	79.7 d	3.52, t (9.2)
5′	77.4 d	3.29, m	77.6 d	3.29[b]	76.8 d	3.31, m
6′	62.63 t	3.84, dd (12.0, 2.2) 3.64[b]	62.62 t	3.84, dd (12.0, 2.3) 3.64, dd (11.9, 5.6)	62.0 t	3.79, m 3.64, m
	2′-*O*-Rha		3′-*O*-Xyl		4′-*O*-Rha	
1″	102.5 d	5.23, s	106.0 d	4.49, d (7.6)	102.9 d	4.84, s
2″	72.1 d	3.96, dd (3.4, 1.7)	75.3 d	3.26, m	72.4 d	3.83, dd (3.4, 1.8)
3″	72.3 d	3.61, m	77.7 d	3.29[b]	72.2 d	3.61, m
4″	73.9 d	3.38, m	71.0 d	3.51, m	73.7 d	3.40, m
5″	69.9 d	4.11, m	67.1 t	3.89, dd (11.4, 5.3) 3.24, m	70.7 d	3.95, m
6″	18.1 q				17.8 q	
				1.23, d (6.1)		1.26, d (6.2)
	3′-*O*-Xyl					
1‴	105.4 d	4.39, d (7.7)				
2‴	74.8 d	3.24, m				
3‴	78.0 d	3.30, m				
4‴	70.9 d	3.51, m				
5‴	67.1 t	3.91, dd (11.5, 5.5) 3.26, m				

[a] Data were recorded at 150 MHZ for ^{13}C NMR and 600 MHz for ^{1}H NMR.
[b] Overlapped.

upper-field shifted with regard to the corresponding signals of the known compounds, pimpifolidine [H_3-18 (δ_H 1.05)], 22-isopimpifolidine [H_3-18 (δ_H 1.09)], but much the same as that of 3-deamino-3β-hydroxysolanocapsine [H_3-18 (δ_H 0.76)], isolated from *Solanum pimpinellifolium* L. (Ripperger, 1994) and *S. aculeatum* Jacq. (Coll et al., 1983), thus demonstrating a 16α-oxygen bridge and a β-oriented OMe-16 (Fig. 1), as determined for 3-deamino-3β-hydroxysolanocapsine (Ripperger, 1994). It is reported that the hitherto characterized solanocapsine type natural alkaloids possess a 16α-oxygen function (Ripperger, 1994). Based on the above evidences, the structure of solanindioside A (**1**) was thus determined as 16β-methoxy-23-deoxy-22,26-epimino-cholest-5,22(28),23,25-tetraen-3-*O*-α-L-rhamnopyranosyl-(1→2)-*O*-[β-D-xylopyranosyl-(1→3)]-β-D-glucopyranoside.

Solanindioside B (**2**) was isolated as a white amorphous powder, positive to Dragendorff test. Its HRESIMS spectrum showed a molecular formula of $C_{39}H_{57}NO_{12}$, on the basis of a protonated molecular ion peak at m/z 732.3955 $[M + H]^+$, (calcd for $C_{39}H_{58}NO_{12}$, 732.3954). The IR spectrum of **2** displayed absorption bands identical to those of **1**. The ^{1}H and ^{13}C NMR spectra (Table 1) of **2** were closely similar to those of **1** except that the ^{13}C NMR signals of **2** were 39 in total, while **1** showed 45 signals. The missing 6 signals in **2** were attributable to a loss of a hexosyl sugar unit. The ^{1}H NMR spectrum of **2** showed two anomeric signals at δ_H 4.43 (1H, d, $J = 7.9$ Hz) and 4.49 (1H, d, $J = 7.6$ Hz), suggesting that **1** possessed two sugar moieties ascribable to one hexosyl and one pentosyl units which, based on J values (Kasai et al., 1979; Ripperger, 1996) and acidic hydrolysis, followed by GC analysis of the corresponding trimethylsilylated L-cysteine adduct, were determined to be β-D-glucosyl and β-D-xylosyl units, respectively. The HMBC correlations, from the xylosyl H-1" (δ_H 4.49) to the glucosyl C-3' (δ_C 87.9) commissioned the determination of the sugar moiety as β-D-xylopyranosyl-(1→3)-β-D-glucopyranoside, from the glucosyl H-1' (δ_H 4.43) to the aglycone C-3 (δ_C 79.7), established the C-3 glycosylation. Based on the above evidences, the structure of solanindioside B (**2**) was thus determined as 16β-methoxy-23-deoxy-22,26-epimino-cholest-5,22(28),23,25-tetraen-3-*O*-β-D-xylopyranosyl-(1→3)-β-D-glucopyranoside.

Solanindioside C (**3**) was afforded as a white amorphous powder, positive to Dragendorff test, and showed a molecular formula of $C_{40}H_{59}NO_{12}$, in reference to the molecular ion peak at m/z 746.4110 $[M + H]^+$ in the HRESIMS (calcd for $C_{40}H_{60}NO_{12}$, 746.4110). The IR spectrum showed absorption bands identical to those of **1**. The ^{1}H and ^{13}C NMR spectra data (Table 1) were closely similar to those of **2** except that the ^{13}C NMR signals of **3** were 40 in total, while in **2** there were 39 signals. The extra single carbon signal in **3** was consigned to a hexosyl sugar unit, instead of a pentosyl sugar unit in **2**. The ^{1}H NMR spectrum of **3** displayed two anomeric protons at δ_H 4.40 (1H, d, $J = 7.9$ Hz) and 4.84 (1H, s), indicating that **3** constituted of two sugar moieties which, on the basis of ^{13}C NMR chemical shift resonances, J values of the anomeric protons (Kasai et al., 1979; Ripperger, 1996) and acidic hydrolysis, followed by GC

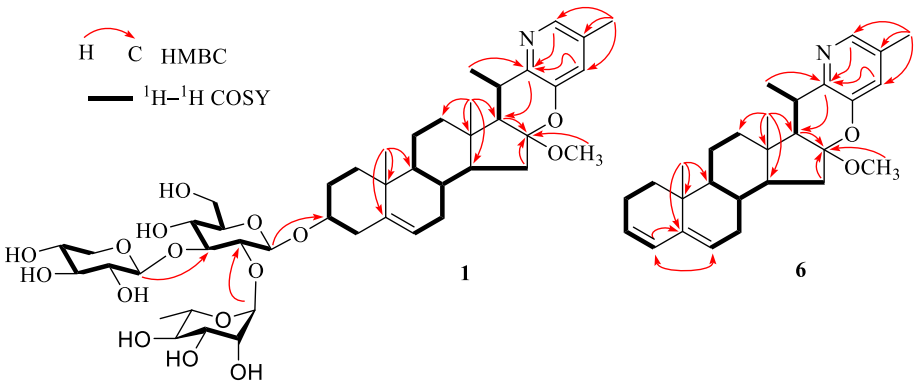

Fig. 2. Key ^{1}H–^{1}H COSY and HMBC correlations of 1 and 6.

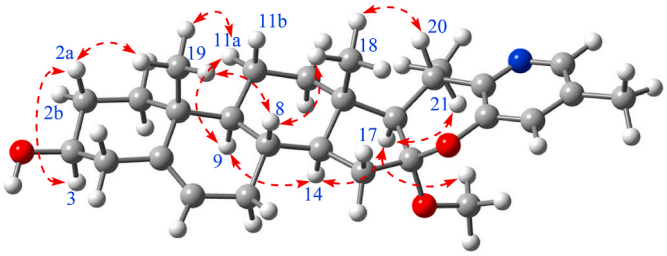

Fig. 3. Key ROESY correlations for the aglycone moiety of 1.

analysis of the corresponding trimethylsilylated L-cysteine adduct, were established to be *β*-D-glucosyl and *α*-L-rhamnosyl units. The *α*-L-rhamnosyl moiety was attached to the glucosyl at C-4' (δ_C 79.7), as demonstrated by HMBC correlations from H-1" (δ_H 4.84) to δ_C 79.7. Furthermore, the HMBC correlation was observed from the glucosyl H-1' (δ_H 4.40) to C-3 (δ 79.8) of the aglycone moiety, to ascertain the C-3 glycosylation. Essentially, these correlations guided the assignment of the glycosidic moiety as *α*-L-rhamnopyranosyl-(1→4)-*O*-*β*-D-glucopyranoside. Subsequently, the structure of solanindioside C (**3**) was elucidated as 16*β*-methoxy-23-deoxy-22,26-epimino-cholest-5,22 (28),23,25-tetraen-3-*O*-*α*-L-rhamnopyranosyl-(1 → 4)-*O*-*β*-D-glucopyranoside.

(22*R*,23*S*,25*R*,26*R*)-spirost-5-ene-3*β*,23,26-triol 3-*O*-*β*-D-xylopyranosyl-(1→3)-*β*-D-glucopyranoside (**4**) was obtained as a white amorphous powder with a molecular formula established as $C_{38}H_{60}O_{14}$, in reference to a sodium adduct molecular ion peak at *m/z* 763.3878 $[M + Na]^+$ in the HRESIMS (calcd for $C_{38}H_{60}O_{14}Na$, 763.3875). The ^{1}H and ^{13}C NMR spectra (Table 2) of the aglycone of **4**, and the hexosyl sugar moiety at δ_H 4.49 (1H, d, J = 7.6 Hz) showed signals quite similar with those of (22*R*,23*S*,25*R*,26*R*)-spirost-5-ene-3*β*,23,26-triol 3-*O*-*α*-L-rhamnopyranosyl-(1→4)-*β*-D-glucopyranoside, previously isolated from the title plant by our research group (Kaunda and Zhang, 2020). However, the signals due to the terminal sugar moiety varied; the ^{1}H NMR displayed its signals at δ_H 4.43 (1H, d, J = 7.9 Hz), and the respective ^{13}C and DEPT signals were observed as a pentosyl unit (106.0, 75.2, 77.7, 69.9 and 67.1), further resolved to be D-xylosyl by acid hydrolysis and subsequent GC analysis of the corresponding trimethylsilylated L-cysteine adduct. The HMBC experiment showed correlations from δ_H 1.17 (H_3-27) to δ_C 67.6 (C-23), 39.7 (C-25) and 96.4 (C-26), from δ_H 1.32 (H_3-21) to δ_C 63.2 (C-17), 37.6 (C-20) and 113.7 (C-22) and from δ_H 4.02 (1H, dd, J = 4.9, 7.8 Hz, H-23) to C-22 (Fig. 4), implying that the aglycone of **4** was a 3,23,26-trihydroxyspirost-5-ene derivative (Mona et al., 2009), even as confirmed by the ^{1}H–^{1}H COSY, HMBC and ROESY correlations (Fig. 4). The H-26 signal appeared as a doublet at δ_H 5.21 (J = 8.0 Hz), expressing *trans*-diaxial coupling between H-26 and H-25 (Mona et al., 2009). Moreover, in the ROESY spectrum, correlations were observed between H-20 (δ 3.03) and H-23 (δ 4.02) as well as between H-23 and H-25 (δ 1.98) (Fig. 4), intimating that C-22 and C-25 were both in the *R* configuration (Mona et al., 2009; Yahara et al., 1996). The HMBC correlations were observed from the xylosyl H-1 (δ 4.43) to glucosyl C-3 (δ 87.9) and from the glucosyl H-1 (δ_H 4.49) to the aglycone C-3 (δ 79.8), as indicated in Fig. 4. The structure of **4** was eventually elucidated as (22*R*,23*S*,25*R*,26*R*)-spirost-5-ene-3*β*,23,26-triol 3-*O*-*β*-D-xylopyranosyl-(1→3)-*β*-D-glucopyranoside.

Table 2
^{13}C and ^{1}H NMR data for **4** in CD_3OD (δ in ppm)[a].

No.	δ_C	δ_H (J in Hz)	No.	δ_C	δ_H (J in Hz)
1	38.5 t	1.71, m; 0.98, m	20	37.0 d	3.03, m
2	30.7 t	2.12, m; 1.76, m	21	14.4 q	1.32, d (6.8)
3	79.8 d	3.98[b]	22	113.7 s	
4	39.7 t	2.73, m; 2.42, m	23	67.6 d	4.02, m
5	142.0 s		24	38.5 t	2.18, m; 2.02, m
6	122.6 d	5.29, d (5.1)	25	39.7 d	1.98, m
7	32.6 t	1.99, m; 1.48, m	26	96.4 d	5.21, d (8.0)
8	32.7 d	1.50, m	27	17.0 q	1.17, d (6.1)
9	51.7 d	0.89, m	1′	102.1 d	4.49, d (7.6)
10	38.0 s		2′	74.4 d	4.07, m
11	22.0 t	1.43, m	3′	87.9 d	4.32, m
12	41.2 t	1.77, m; 1.14, m	4′	70.9 d	4.30, m
13	41.9 s		5′	77.6 d	3.98[b]
14	57.8 d	1.07 m	6′	62.6 t	4.57, m; 4.43, m
15	33.2 t	2.01, m; 1.81, m	1″	106.0 d	4.43, d (7.9)
16	82.8 d	4.71, m	2″	75.2 d	3.20, m
17	63.2 d	1.96, m	3″	77.7 d	3.28, m
18	17.0 q	1.03, s	4″	69.9 d	3.49, m
19	19.9 q	0.86, s	5″	67.1 t	3.88, dd (11.5, 5.5)
					3.24, m

[a] Data were recorded at 150 MHZ for ^{13}C NMR and 600 MHz for ^{1}H NMR.
[b] Overlapped.

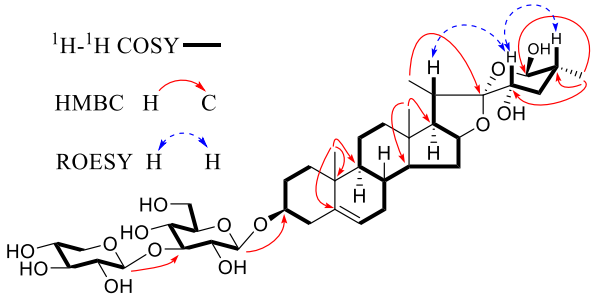

Fig. 4. Key ^{1}H–^{1}H COSY, HMBC, ROESY correlations of 4.

Solanindin A (**5**), a white amorphous powder, showed a molecular formula of $C_{28}H_{39}NO_3$, according to the protonated molecular ion peak at *m/z* 438.3005 $[M + H]^+$ in the HRESIMS (calcd for $C_{28}H_{40}NO_3$, 438.3003). The IR spectrum expressed absorption bands identical to those of **1**. The ^{1}H NMR spectrum of **5** (Table 3) showed two tertiary methyls at δ_H 0.57 and 1.02 (each 3H, s, CH_3-18, CH_3-19), two

secondary methyls at δ_H 1.47 (3H, d, $J = 7.2$ Hz, CH_3-21) and δ_H 2.31 (3H, s, CH_3-27), three olefinic signals at δ_H 5.35 (1H, br. d, $J = 5.0$ Hz, H-6), 7.51 (1H, s, H-24), 7.11 (1H, s, H-26), and one methoxy group at δ_H 3.18. The ^{13}C NMR and DEPT spectra of **5** (Table 3) showed a total of 28 signals, comprising an oxygenated methine [δ_C 72.3 (C-3), three tri-substituted double bonds [δ_C 121.8 (C-6), 120.3 (C-24), 134.7 (C-26)], seven methylenes [δ_C 38.4 (C-1), 32.2 (C-2), 42.9 (C-4), 32.9 (C-7), 21.5 (C-11), 40.6 (C-12), and 39.6 (C-15)], five methines [δ_C 32.3 (C-8), 51.3 (C-9), 55.5 (C-14), 62.59 (C-17), 36.0 (C-20)], four methyls (δ_C 14.1 (C-18), 19.8 (C-19), 18.3 (C-21), 18.2 (C-27), one methoxy moiety (δ_C 52.5), and seven quaternary carbons [δ_C 142.1 (C-5), 37.8 (C-10), 44.9 (C-13), 151.0 (C-22), 116.2 (C-16), δ_C 165.1 (C-23), and 139.6 (C-25)], assignable to the aglycone. The structure of **5** was assembled by employing the HMBC correlations, as described in **1** above, and the observations, exactly similar to those of **1**, further confirmed the structure of the aglycone of **1**. Based on the above pieces of evidence, the structure of solanindin A (**5**) was determined as 16β-methoxy-23-deoxy-22,26-epimino-cholest-5,22(28),23,25-tetraen.

Solanindin B (**6**) was obtained as a white amorphous powder. Its molecular formula was determined as $C_{28}H_{37}NO_2$ based on an ion peak at m/z 420.2899 $[M + H]^+$ in the HRESIMS (calcd for $C_{28}H_{38}NO_2$, 420.2897). The IR spectrum of **6** expressed absorption bands identical to those of **1**. With reference to **5**, the ^1H NMR spectrum of **6** (Table 3) showed two more olefinic proton signals at δ_H 5.57 (m), and 5.89 (d, $J =$ 10.0 Hz), which were confirmed by HSQC spectrum to be corresponding to two methine signals at δ_C 125.9 and 130.1, respectively. The ^1H–^1H COSY revealed the linkage between δ_H 1.70/2.10/5.57/5.89 (H-1/H-2/H-3/H-4, resp.). Hence, δ_H 5.57 (m); δ_C 125.9 and δ_H 5.89 (d, $J = 10.0$ Hz); δ_C 130.1 were assigned to C-3 and C-4, respectively (Fig. 2).

Table 3
^{13}C and ^1H NMR data for 5–6 in CD_3OD (δ in ppm)[a].

No.	5		6	
	δ_C	δ_H (J in Hz)	δ_C	δ_H (J in Hz)
1	38.4 t	1.88[b]	34.8 t	1.70, m
		1.08, m		1.16, m
2	32.2 t	1.78, m	23.9 t	2.18, m
		1.47, m		2.09, m
3	72.3 d	3.39, m	125.9 d	5.57, m
4	42.9 t	2.23, m	130.1 d	5.89, d (10.0)
5	142.1 s		142.8 s	
6	121.8 d	5.35, d (5.0)	123.1 d	5.36, d (2.7)
7	32.9 t	2.05, m	32.8 t	1.79, m
		1.64, m		2.25, m
8	32.3 d	1.64, m	32.2 d	1.80, m
9	51.3 d	1.08, m	52.5 d	3.19, s
10	37.8 s		36.4 s	
11	21.5 t	1.64, m	21.4 t	1.68, m
		1.50, m		1.44[b]
12	39.6 t	1.94, m	39.6 t	1.95[b]
		1.88[b]		1.44[b]
13	44.9 s		45.0 s	
14	55.5 d	1.52, m	55.8 d	1.52, m
15	40.6 t	2.53, dd (13.1, 5.8)	40.4 t	2.55, dd (13.0, 5.9);
		1.88[b]		1.95[b]
16	116.2 s		116.2 s	
17	62.59 d	2.20, s	62.6 d	2.22, s
18	14.1 q	0.57, s	14.1 q	0.59, s
19	19.8 q	1.02, s	19.1 q	0.95, s
20	36.0 d	3.56, dd (14.6, 7.3)	36.0 d	3.58, dd (14.5, 7.4)
21	18.3 q	1.47, d (7.2)	18.3 q	1.47, d (7.3)
22	151.0 s		151.0 s	
23	165.1 s		165.1 s	
24	120.3 d	7.51, s	120.3 d	7.51, s
25	139.6 s		139.6 s	
26	134.7 d	7.11, s	134.7 d	7.11, s
27	18.2 q	2.31, s	18.2 q	2.31, s
OMe	52.5 q	3.18, s	52.5 q	3.18, s

[a] Data were recorded at 150 MHz for ^{13}C NMR and 600 MHz for ^1H NMR.
[b] Overlapped.

Moreover, in HMBC spectrum, correlations were observed from δ_H 5.36 (H-6) to δ_C 130.1 (C-4), as well as from δ_H 5.89 (H-4) to δ_C 142.8 (C-5) and 123.1 (C-6), as shown in Fig. 2. The introduction of a double bond between C-3 and C-4 indicated that compound **5** lost H_2O molecule at C-3. Solanindin B (**6**) was thus elucidated as 16β-methoxy-3,23-dideoxy-22,26-epimino-cholest-3,5,22 (28),23,25-pentaen.

2.2. Cytotoxic, apoptotic and antibacterial activity

In view of various reports of cytotoxic and antibacterial effects of *Solanum* alkaloids (Kaunda and Zhang, 2019a), we evaluated compounds **1**–**6** for the biological activities mentioned above. Moreover, due to the impressive antitumor effects demonstrated by lignans (Cutillo et al., 2003), and considering that previous reports (Cutillo et al., 2003; Khan et al., 2020; Niemi et al., 2012; Smeds et al., 2007, 2012; Della-Greca et al., 2006; Honbu et al., 2002) on compound **9**, a lignan, did not illuminate on its biological activities, we undertook to evaluate its cytotoxic efficacy, alongside the formerly undescribed isolates.

Compounds **1**–**6** and **9** were tested for their cytotoxicity on four human cancer (human leukemia HL-60, lung cancer A549, breast cancer MCF-7 and colon cancer SW480) cell lines by MTS method. The results of preliminary evaluation at 40 μM showed that **1–5** were not active against all the cancer cell lines. The inhibition rate of compound **6** on the growth of SMMC-7721 and MCF-7 were greater than 50%, and thus it was further evaluated for its IC_{50} effects. The results showed that **6** exhibited some potency against SMMC-7721 ($IC_{50} = 29.71 \pm 1.80$) and MCF-7 ($IC_{50} = 29.93 \pm 0.92$) cell lines (Table 4). Compound **9** demonstrated strong cytotoxic potency against MCF-7, with an IC_{50} value of 4.386 ± 0.098 μM (Table 4).

Since compound **9** showed substantial cytotoxic potential, it was further tested for its cell apoptosis activity in MCF-7 cells. Apoptosis is a programmed cell death whose favorable results could be applied to bombard tumors (Zhang et al., 2018). Compound **9** slightly induced apoptosis in the tumor microenvironment by repressing cell proliferation. The outcome indicated that it induced apoptosis in MCF-7 cells at the rate of 21.14 and 26.84% at concentrations of 10 and 15 μM (Fig. 5), respectively.

The antibacterial activity of compounds **1**–**6** on *Escherichia coli* Migula, *Staphylococcus aureus* subsp. *aureus*, *Salmonella enterica* subsp. *enterica* (*ex* Kauffmann and Edwards), and *Pseudomonas aeruginosa* Migula was investigated using MH and LB broth media. At a concentration of 200 μM, **6** showed significant inhibitory effects (99.94%) against *S. aureus* (Table S4, Supplementary data), thus was further tested for its MIC_{50} (50% minimum inhibitory concentration) on *S. aureus*, and the result was calculated by Reed & Muench method; it displayed MIC_{50} value of 37.32 ± 0.793 μM (Table S5, Supplementary data).

It is interesting that **6**, a by-product from acid hydrolysis, exhibited better biological activity than **1**–**3** and **5**. Based on the structural features of **1–3** and their bioassay test results, the structure-activity relationships (SAR) of **1**–**3** could be contemplated as follows: By comparing **1**–**3** with **6**, it could be deduced that the presence of the sugar moieties in **1–3** considerably hindered their biological activity;

Table 4
Cytotoxic activities ($IC_{50} \pm$ SD (μM)) of 6 and 9.

Compounds	HL-60	A549	SMMC-7721	MCF-7	SW480
6	–	–	29.71 ± 1.80	29.93 ± 0.92	–
9	8.25 ± 0.39	15.13 ± 0.81	10.63 ± 0.15	4.386 ± 0.098	16.12 ± 1.46
DDP (cisplatin)[a]	3.45 ± 0.50	28.19 ± 0.80	14.30 ± 0.16	9.98 ± 0.58	11.08 ± 0.81
Taxol (paclitaxel)[a]	<0.008	<0.008	<0.008	<0.008	<0.008

[a] Positive control; –: no activity at 40 μM.

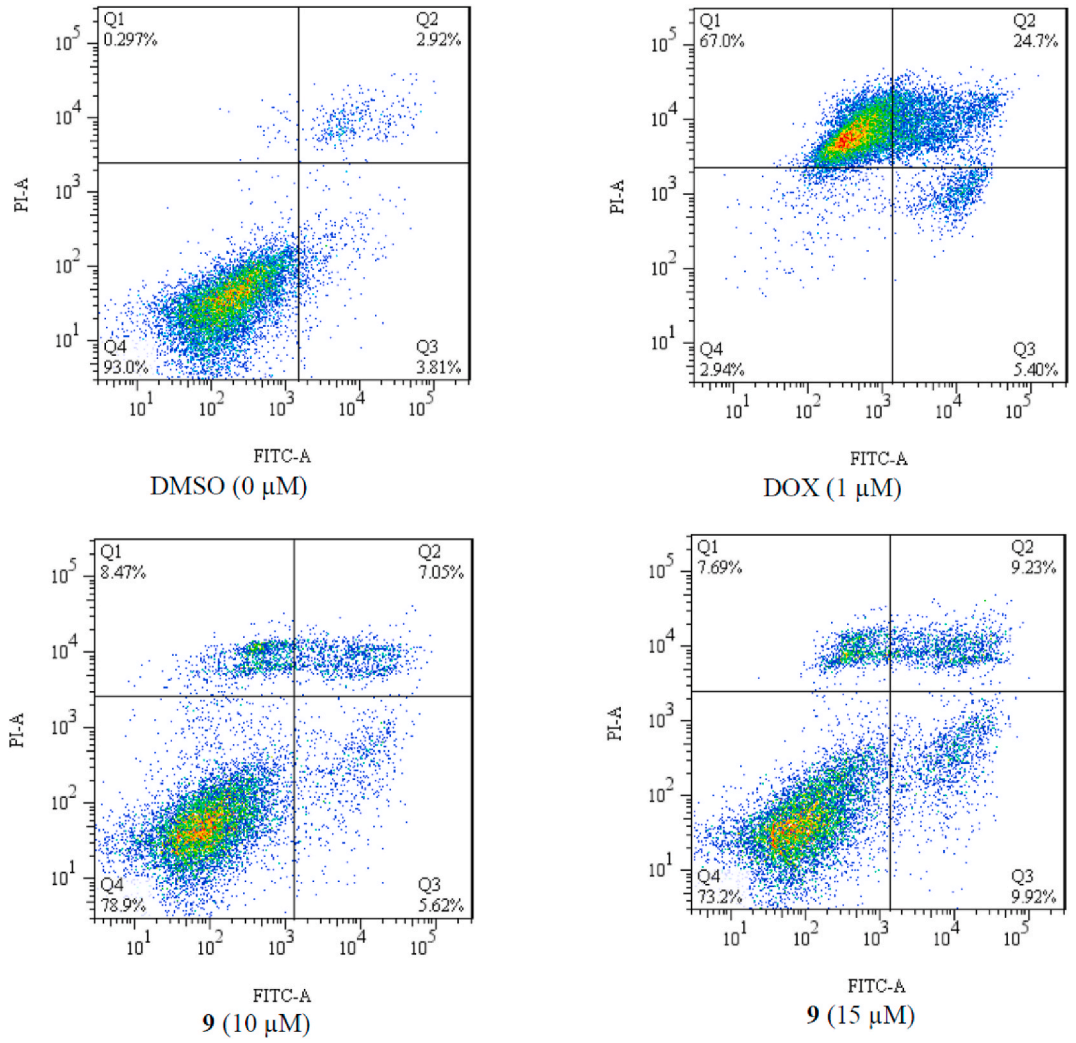

Fig. 5. Apoptosis induced by **9** in MCF-7 cells. [Q3: The early stage of apoptosis (FITC positive, PI negative) Q2: The late stage of apoptosis (FITC positive, PI positive) Q4: The live cells (FITC negative, PI negative)].

comparison of **5** and **6** indicate that the presence of a hydroxy group at C-3 of **5** could have inhibited its biological efficacy. Therefore, further structural modification of **6** may additionally unlock and enhance its biological potency.

3. Conclusion

Our studies on the fruits of *S. violaceum* resulted in the isolation of three previously undescribed pyridyl-type steroidal alkaloids of the solanocardinol derivative (**1**–**3**) (Osman et al., 1991), one rare 23*S*, 26*R*-hydroxylated spirostanoid saponin, a type previously isolated only from the title plant (Kaunda and Zhang, 2020), *S. indicum* L. (Mona et al., 2009) and *S. anguivi* Lam. (Nafady et al., 2003; Honbu et al., 2002), together with five known compounds (**5**–**9**). Among the known compounds, **9** was obtained for the first time from the Solanaceae family, hence expanding its chemical scope. Compound **9** displayed strong cytotoxic activity.

4. Experimental

4.1. General experimental procedures

The instruments and the chromatographic materials and equipment were similar with those reported previously (Kaunda and Zhang, 2019b, 2020] but with some alterations.

IR spectra were measured on a Bio-Rad FTS-135 series spectrometer with KBr pellets. Optical rotations were measured on Rudolph Autopol VI polarimeter (Rudolph Research Analytical, Hacketstown, NJ, USA). UV spectra were recorded on a UV 210A Shimadzu spectrometer. CD spectra were obtained on a JASCO 810 spectrometer. One- and two-dimensional (1D and 2D) NMR spectra were recorded in methanol-d_4 with Bruker DRX-600 operating at 600 MHz for ^{1}H and at 150 MHz for ^{13}C. Coupling constants are expressed in hertz, and chemical shifts are given on a δ (parts per million, ppm) scale with tetramethylsilane (TMS) as an internal standard. ESI mass spectra were recorded on a VG Auto Spec-300 spectrometer. High-resolution (HR) ESI mass spectra were recorded on an API QSTAR Pular-1 spectrometer. Column chromatography (CC) was performed on MCI gel CHP20P (75–100 μm, Mitsubishi Chemical Co., Ltd.), and silica gel (200–300 mesh, Qingdao Marine Chemical Co., Qingdao, China). Preparative HPLC and semi-preparative reversed-phase were performed using a Capcell C18 (Agilent, America) column (10 mm × 250 mm) and Cosmosil cholester (Kyoto, Japan) column (4.6 mm I.D. × 150 mm); the flow rate used for Preparative HPLC was 3.0 mL/min, and the separation and detection were achieved using Newstyle NU3000 SERIALS UV/VIS detector (Jiangsu Hanbon Science & Technology Co. Ltd, China). Thin-layer chromatography (TLC) was performed on precoated silica gel H plates, 0.20–0.25 mm thick (Qingdao Haiyang Chemical Co.), with chloroform/methanol/water (7:3:0.5 or 8:2:0.2 v/v/v), and spots were visualized under UV light and by spraying with 10% H_2SO_4 in EtOH followed by heating.

Water was purified in a Milli-Q (Millipore, America). Acetonitrile (chromatographic grade) was purchased from Merck (Darmstadt, FR). MH broth and LB broth were purchased from Guangdong Huankai Microbiology Technology Co., Ltd. Penicillin G Sodium was purchased from Biosharp, Ceftazidime was purchased from Shanghai Yuanye Biotechnology Co., Ltd.

4.2. Plant material

Ripe fruits of *Solanum violaceum* Ortega (Solanaceae, synonym *Solanum indicum* var. *recurvatum*) were collected in December 2018 in the vicinity of Xiding township, Menghai county, Xishuangbanna, Yunnan province, China (Latitude: 21.959883 | Longitude: 100.451189). The plant material was identified by Prof. C.-R. Yang and a voucher specimen (KIB-Z-2018012) was deposited in the State Key Laboratory of Phytochemistry and Plant Resources in West China, Kunming Institute of Botany, Chinese Academy of Sciences, Kunming, China, even as previously reported (Kaunda and Zhang, 2020).

4.3. Extraction and isolation

Dried fruits (1.5 kg) of *S. violaceum* were crushed into powder and extracted in a Soxhlet apparatus with methanol for 72 h. The methanol extract (4.5 L) was then concentrated in a rotary evaporator to give a residue (122 g) which was suspended in water (1000 mL) and extracted with *n*-butanol (each 500 mL, 4 times) to yield *n*-butanol (63 g) and water (45 g) fractions. The *n*-butanol fraction (63 g) was subjected to MCI gel, eluting with MeOH: H_2O (0:1 → 1:0), to give 7 fractions, M1-M7.

Fraction M2 (15.5 g) was applied to silica gel (300 g) column (4.0 × 35 cm), eluting with chloroform/methanol/water (100:0:0, 98:2:0, 96:4:0, 94:6:0, 92:8:0, 90:10:0, 90:10:1, 85:15:1, 80:20:2 v/v) to generate 6 fractions, M2a-M2f. Fractions, M2c (1.1 g), M2d (1.2 g) and M2e (900 mg) were submitted for further purification by preparative HPLC with an isocratic mobile phase system of acetonitrile/water (24:76, v/v). Fraction M2c gave **4** (t_R = 38 min, 6.0 mg); 26:74, v/v)]. Fraction M2d provided **3** [t_R = 68 min, 16.0 mg and **2** (t_R = 78 min, 24.0 mg); 13:87, v/v]. Fraction M2e furnished **1** [t_R = 15 min, 12.0 mg, **8** (t_R = 25 min, 10.0 mg, and **7** (t_R = 34 min, 6.0 mg)].

Fraction M6 (6 g) was applied to silica gel CC (120 g, 4.0 × 30 cm), eluting as aforementioned to afford fractions M6a-M6h. Fraction M6h (850 mg) was applied to silica gel CC (120 g, 4.0 × 30 cm), eluted as before, to offer two fractions, M6h-1 (120 mg) and M6h-2 (140 mg), which were further purified by preparative HPLC using an isocratic mobile phase system of acetonitrile/water (39:61, v/v). M6h-1 (120 mg) yielded **11** [t_R = 65 min, 4.0 mg) and **9** (t_R = 74 min, 4.0 mg (18:82, v/v)]. M6h-2 (140 mg) gave **10** [t_R = 60 min, 4.0 mg].

4.3.1. Solanindioside A (1)

White amorphous powder; $[\alpha]_D^{21}$ −134 (*c* 0.1, MeOH); UV (MeOH) λ_{max} (log ε) 202 (0.31), 225 (0.30), 260 (0.08), and 330 (0.10) nm; IR (KBr) ν_{max} 3424, 2934, 2852, 1632, 1588, 1563, 1453, 1435, 1384, 1365, 1334, 1299, 1245, 1203, 1126, 1044 cm^{-1}; ECD (MeOH) λ_{max} ($\Delta\varepsilon$) 211 (+2.90), 231 (−4.65), and 263 (+0.91); HRESIMS *m/z*: 878.4536 $[M + H]^+$ (calcd for $C_{45}H_{68}NO_{16}$, 878.4533); for ^1H and ^{13}C NMR (600/150 MHz, CD_3OD) data, see Table 1.

4.3.2. Solanindioside B (2)

White amorphous powder; $[\alpha]_D^{22}$ −65 (*c* 0.1, MeOH); UV (MeOH) λ_{max} (log ε) 202 (0.26), 226 (0.38), 260 (0.11), and 331 (0.15) nm; IR (KBr) ν_{max} 3419, 2967, 2935, 2904, 2852, 1633, 1585, 1562, 1477, 1453, 1435, 1384, 1363, 1333, 1298, 1273, 1245, 1201, 1156, 1121, 1084, 1044 cm^{-1}; ECD (MeOH) λ_{max} ($\Delta\varepsilon$) 211 (+4.56), 231 (−6.04), and 262 (+1.68); HRESIMS *m/z*: 732.3955 $[M + H]^+$ (calcd for $C_{39}H_{58}NO_{12}$, 732.3954); for ^1H and ^{13}C NMR (600/150 MHz, CD_3OD) data, see Table 1.

4.3.3. Solanindioside C (3)

White amorphous powder; $[\alpha]_D^{21}$ −85 (*c* 0.1, MeOH); UV (MeOH) λ_{max} (log ε) 202 (0.38), 226 (0.49), 261 (0.14), and 331 (0.18) nm; IR (KBr) ν_{max} 3423, 2934, 2852, 1632, 1584, 1562, 1478, 1453, 1384, 1363, 1334, 1298, 1274, 1258, 1244, 1200, 1121, 1064, 1040 cm^{-1}; ECD (MeOH) λ_{max} ($\Delta\varepsilon$) 211 (+5.02), 230 (−5.74), and 263 (+2.01); HRESIMS *m/z*: 746.4110 $[M + H]^+$ (calcd for $C_{40}H_{60}NO_{12}$, 746.4110); for ^1H and ^{13}C NMR (600/150 MHz, CD_3OD) data, see Table 1.

4.3.4. (22R,23S,25R,26R)-spirost-5-ene-3β,23,26-triol 3-O-β-D-xylopyranosyl-(1 → 3)-β-D-glucopyranoside (4)

White amorphous powder; $[\alpha]_D^{22}$ −39 (*c* 0.1, MeOH); UV (MeOH) λ_{max} (log ε) 202 (0.33), 270 (0.01) nm; IR (KBr) ν_{max} 3419, 2935, 2903, 2847, 1633, 1454, 1435, 1414, 1384, 1383, 1274, 1249, 1198, 1156, 1067, 1042 cm^{-1}; ECD (MeOH) λ_{max} ($\Delta\varepsilon$) 198 (+5.60); HRESIMS *m/z*: 763.3878 $[M + Na]^+$ (calcd for $C_{38}H_{60}O_{14}Na$, 763.3875); for ^1H and ^{13}C NMR (600/150 MHz, CD_3OD) data, see Table 2.

4.3.5. Acid hydrolysis of compounds 1–3

A mixture of compounds **1**–**3** (56 mg) was dissolved in 5% HCl (8 mL) and heated (90 °C) for 2 h. HCl was then removed by evaporation in vacuum. The reaction mixture was diluted with H_2O and extracted with $CHCl_3$. The $CHCl_3$ layer was dried to afford aglycone (24 mg), which was submitted for ^1H and ^{13}C NMR (600/150 MHz, CD_3OD). The 1D NMR spectra revealed a mixture of two compounds which were further separated by preparative HPLC with an isocratic mobile phase system of acetonitrile/water (80/20, v/v) to bring forth compounds **5** (t_R = 11.2 min, 4.0 mg) and **6** (t_R = 16 min, 2.0 mg).

4.3.5.1. Solanindin A (5). White amorphous powder; $[\alpha]_D^{21}$ +16 (*c* 0.1, MeOH); UV (MeOH) λ_{max} (log ε) 196 (0.56), 256 (0.03), 270 (0.03), 301 (0.02), and 328 (0.02) nm; ECD (MeOH) λ_{max} ($\Delta\varepsilon$) 210 (+0.51), and 228 (−0.26); HRESIMS *m/z*: 438.3005 $[M + H]^+$ (calcd for $C_{28}H_{40}NO_3$, 438.3003); for ^1H and ^{13}C NMR (600/150 MHz, CD_3OD) data, see Table 3.

4.3.5.2. Solanindin B (6). White amorphous powder; $[\alpha]_D^{20}$ −42 (*c* 0.1, MeOH); UV (MeOH) λ_{max} (log ε) 198 (0.38), 228 (0.82), and 331 (0.15) nm; IR (KBr) ν_{max} 3426, 3017, 2968, 2935, 2872, 2852, 1665, 1651, 1631, 1584, 1561, 1478, 1453, 1384, 1362, 1334, 1299, 1266, 1244, 1220, 1202, 1176, 1154, 1143, 1122, 1088, 1068, 1044 cm^{-1}; ECD (MeOH) λ_{max} ($\Delta\varepsilon$) 211 (+5.02), 230 (−5.74), and 263 (+2.01); HRESIMS *m/z*: 420.2899 $[M + H]^+$ (calcd for $C_{28}H_{38}NO_2$, 420.2897); for ^1H and ^{13}C NMR (600/150 MHz, CD_3OD) data, see Table 3.

4.4. Acid hydrolysis of compounds 1–4 and GC analysis

The procedure was as hitherto described (Kaunda and Zhang, 2020), with minimum modifications. Compounds **1**–**3** (56 mg) were dissolved in 5% HCl (8 mL) and heated (90 °C) for 2 h. The HCl was then removed by evaporation in vacuum. The reaction mixture was diluted with H_2O and extracted with $CHCl_3$. The aqueous layer was neutralized with 0.1 M NaOH and dried to give the monosaccharide mixture. Into the solution of the sugar mixture in pyridine (2 mL) was added L-cysteine methyl ester hydrochloride (about 3 mg) and the reaction mixture kept at 60 °C for 1 h before addition of trimethylsilylimidazole (4 mL) in to the mixtures. Following this, the reaction mixture was further kept at 60 °C for 1 h, before stopping the reaction and immediately submitting them for GC analysis [5], run on Hewlett Packard (HP) 5890 series II gas chromatography equipped with flame ionization detector (FID) and thermal conductivity detector (TCD). The column was HP-5: column temperature: 280 °C, increasing at the rate of: 3 °C/min; carrier gas: N_2 (1.5 mL/min); injector and detector temperature: 250 °C; injection volume:

1.0 μL; and split ratio: 1/100. The retention times of the samples were compared with those of the derivatives of authentic sugars, under the same condition. The sugar moieties were determined to be D-glucose (t_R: 30.073 min), D-xylose (t_R: 25.940 min), and L-rhamnose (t_R: 23.757 min) by crosschecking with the standards, D-glucose (t_R: 29.705 min), D-xylose (t_R: 26.148 min), and L-rhamnose (t_R: 23.865 min), respectively. Separately, compound **4** was subjected to the same procedure. The sugar moieties of **4** were determined as D-glucose (t_R: 28.321 min) and D-xylose (t_R: 25.987 min), by comparing with the standards, D-glucose (t_R: 29.705 min), D-xylose (t_R: 26.148 min), respectively (Fig. S51-53, Supplementary data).

4.5. Cytotoxic activities assay

Compounds **1**–**6** and **9** were evaluated against four human cancer (human leukemia HL60, lung cancer A549, breast cancer MCF-7 and colon cancer SW480) by MTS method in 96-well microplates as previously described (Kaunda and Zhang, 2020). Having displayed growth inhibition rates of 50%, compounds **6** and **9** were further evaluated at concentrations of 0.064, 0.32, 1.6, 8, and 40 μM in triplicate, with cisplatin (DDP) and taxol as positive controls. Cell growth curve was plotted with the concentration as abscissa and cell viability as ordinate. The optical density (OD) was measured at 492 nm using MULTISKAN FC to determine inhibition rates. The IC_{50} values were determined by Reed and Muench method (Reed et al., 1938).

4.6. Flow cytometry assay for apoptosis

The apoptosis effect of compound **9** in MCF-7 cells was determined using a procedure described before (Qin et al., 2020). Flow cytometry was used to analyze the effect of **9** on the apoptosis of MCF-7 cancer cells. Cells were seeded into 6-well plates (3×10^6/well) in 10% fetal bovine serum (FBS)-RMPI1640 to the final volume of 2.0 mL. After being cultured all night long, cells were treated with different concentrations (1, 10, and 15 μM) of **9**, and incubated for 24 h. Doxorubicin was used as the positive control. The cells were digested with trypsin and washed twice with cold PBS, then collected and re-suspended in binding buffer at a concentration of 1×10^6 cells/mL. In to 100 μL of the PBS solution, 5.0 μL of FITC Annexin V (BD, Pharmingen) and 5.0 μL PI were added, then annexin-V FITC apoptosis kit was used; the cells were gently vortexed and incubated for 30 min at room temperature in a dark place. The apoptotic experiment was analyzed using the flow cytometry (BD, FACSCelesta, America).

4.7. Antibacterial activities assay

The inocula of the bacterial strains prepared from 24 h-old cultures and suspensions were adjusted to 0.5 McFarland standard turbidity. A volume of 100 μL aliquot from the stock solutions of the samples initially prepared was added into the 96-well plates. Then, 100 μL of the inoculums were added to achieve a final inoculum concentration of 5×10^5 CFU/mL. The final volume in each well was 200 μL. After incubation at 37 °C for 24 h, growth was monitored by Microplate Reader at 625 nm. MIC_{50} (50% minimum inhibitory concentration) was calculated by Reed & Muench method (Reed et al., 1938).

Declaration of competing interest

The authors declare that they have no known competing financial interests or personal relationships that could have appeared to influence the work reported in this paper.

Acknowledgements

The authors are grateful to the members of the analytical group at the State Key Laboratory of Phytochemistry and Plant Resources in West China, Kunming Institute of Botany, Chinese Academy of Science, for measuring the spectroscopic data. This work was supported by the National Natural Science Foundation of China (82074124) and the Key Project of Basic Research Plan of Yunnan Province, China (202001AS070017).

Appendix A. Supplementary data

Supplementary data to this article can be found online at https://doi.org/10.1016/j.phytochem.2021.112656.

Web reference

http://www.plantsoftheworldonline.org/taxon/urn:lsid:ipni.org:names:821485-1 (accessed on 21 December 2020.

References

Abdel-Kader, M.S., Bahler, B.D., Malone, M.S., et al., 2000. DNA-damaging steroidal alkaloids from eclipta alba from the Suriname rainforest. J. Nat. Prod. 63, 1184. https://doi.org/10.1021/np000312f.

Augustin, M.M., Ruzicka, D.R., Shukla, A.K., 2015. Elucidating steroid alkaloid biosynthesis in Veratrum californicum: production of verazine in Sf9 cells. Plant J. 82, 991–1003. https://doi.org/10.1111/tpj.12871.

Ayoub, S.M.H., Kingston, D.G.I., 1984. Laricirесinol derivatives from Turrea nilotica and Monechma ciliatum. J. Nat. Prod. 47, 875–876. https://doi.org/10.1021/np50035a023.

Coll, F., Preiss, A., Basterechea, M., Mola, J.L., Adam, G., 1983. 3-Desamino-3α-hydroxysolanocapsine—a steroidal alkaloid from Solanum aculeatum. Phytochemistry 22, 2099–2100. https://doi.org/10.1016/0031-9422(83)80061-2.

Cutillo, F., D'Abrosca, B., DellaGreca, M., et al., 2003. Lignans and neolignans from Brassica fruticulosa: effects on seed germination and plant growth. J. Agric. Food Chem. 51, 6165–6172. https://doi.org/10.1021/jf034644c.

DellaGreca, M., Cutillo, F., D'Abrosca, B., et al., 2006. Isolation of seed germination and plant growth inhibitors from Mediterranean plants: their potential use as herbicides. ACS Symp. Ser. 927, 24–36. https://pubs.acs.org/doi/abs/10.1021/bk-2006-0927.ch002.

Honbu, T., Ikeda, T., Zhu, X.H., et al., 2002. New steroidal glycosides from the fruits of Solanum anguivi. J. Nat. Prod. 65, 1918–1920. https://doi.org/10.1021/np020254t.

Kasai, R., Okihara, M., Asakawa, J., 1979. Carbon- 13 NMR study of α- and β- anomeric pairs of D- mannopyranosides and L- rhamnopyranosides. Tetrahedron 35, 1427–1432. https://doi.org/10.1016/0040-4020(79)85038-3.

Kaunda, J.S., Zhang, Y.J., 2019a. The genus Solanum: an ethnopharmacological, phytochemical and biological properties review. Nat. Prod. Bioprosp. 9, 77–137. https://doi.org/10.1007/s13659-019-0201-6.

Kaunda, J.S., Zhang, Y.J., 2019b. Two new phenolic constituents from the stems of Euphorbia griffithii. Nat. Prod. Biop. 9, 405–410. https://doi.org/10.1007/s13659-019-00223-2.

Kaunda, J.S., Zhang, Y.J., 2020. Two new 23S,26R-hydroxylated spirostanoid saponins from the fruits of Solanum indicum var. recurvatum. Steroids 153, 108506. https://doi.org/10.1016/j.steroids.2019.108506.

Khan, Z.S., Chatterjee, N.S., Shabeer, T.P., et al., 2020. Profile of triacylglycerols, phenols, and vitamin E of manjari medika grape seed oil and cake: introducing a novel Indian variety. Eur. J. Lipid Sci. Technol. 122, 1900356. https://doi.org/10.1002/ejlt.201900356.

Li, D., Zhao, Y.L., Qin, X.J., 2016. Spiralosides A- C, three new C27- steroidal glycoalkaloids from the fruits of Solanum spirale. Nat. Prod. Bioprospect. 6, 225–231. https://doi.org/10.1007/s13659-016-0103-9.

Mona, E.A., Miyashita, H., Ikeda, T., Lee, J.H., Yoshimitsu, H., 2009. A New spirostanol glycoside from fruits of Solanum indicum. L. Chem. Pharm. Bull. 57, 747–748. https://doi.org/10.1248/cpb.57.747.

Nafady, A.M., El-Shanawany, M.A., Mohamed, M.H., et al., 2003. Peculiar side-chain fission of steroidal glycosides. Tetrahedron Lett. 44, 3509–3511. https://doi.org/10.1016/S0040-4039(03)00689-0.

Niemi, P., Tamminen, T., Smeds, A., et al., 2012. Characterization of lipids and lignans in brewer's spent grain and its enzymatically extracted fraction. J. Agric. Food Chem. 60, 9910–9917. https://doi.org/10.1021/jf302684x.

Osman, S.F., Sinden, S.L., Irwin, P., Deahl, K., Tingey, W.M., 1991. Solanocardinol: a steroidal alkaloid from Solanum neocardenasii. Phytochemistry 30, 3161–3163. https://doi.org/10.1016/S0031-9422(00)98282-7.

Qin, X.J., Zhang, L.J., Zhang, Y., et al., 2020. Polyphyllosides A–F, six new spirostanol saponins from the stems and leaves of Paris polyphylla var. chinensis. Bioorg. Chem. 99, 103788. https://doi.org/10.1016/j.bioorg.2020.103788.

Reed, L.J., Muench, H.A., 1938. A simple method of estimating fifty per cent endpoints. Am. J. Hyg. 27, 493–497. https://doi.org/10.1093/oxfordjournals.aje.a118408.

Ripperger, H., Porzel, A., 1994. Pimpifolidine and 22-isopimpifolidine, 22,26-epimino-16,23-epoxycholestane alkaloids from the wild tomato Lycopersicon pimpinellifolium. Phytochemistry 35, 813–815. https://doi.org/10.1016/S0031-9422(00)90612-5.

Ripperger, H., 1996. Steroidal alkaloids from roots of Solanum spirale. Phytochemistry 43, 705–707. https://doi.org/10.1016/0031-9422(96)00347-0.

Satti, N.K., Suri, O.P., Dhar, K.L., et al., 1987. Isolation and characterization of 3-oxoatisane- 16α, 17- diol from Euphorbia acaulis. J. Nat. Prod. 50, 790–793. https://doi.org/10.1016/0031-9422(88)80232-2.

Smeds, A.I., Eklund, P.C., Sjoeholm, R.E., et al., 2007. Quantification of a broad spectrum of lignans in cereals, oilseeds, and nuts. J. Agric. Food Chem. 55, 1337–1346. https://doi.org/10.1021/jf0629134.

Smeds, A.I., Eklund, P.C., Willfor, S.M., Stefan, M., 2012. Content, composition, and stereochemical characterisation of lignans in berries and seeds. Food Chem. 134, 1991–1998. https://doi.org/10.1016/j.foodchem.2012.03.133.

Xu, Y.L., Jia, Lv, Wang, W.F., Liu, Y., Xu, Y.J., Xu, T.H., 2018. New steroidal alkaloid and furostanol glycosides isolated from Solanum lyratum with cytotoxicity. Chin. J. Nat. Med. 16, 499–504. https://doi.org/10.1016/S1875-5364(18)30085-2.

Yahara, S., Nakamura, T., Someya, Y., 1996. Steroidal glycosides, indiosides A-E, from Solanum indicum. Phytochemistry 43, 1319–1323. https://doi.org/10.1016/S0031-9422(96)00395-0.

Zhang, X., Yan, Z., Xu, T., et al., 2018. Solamargine derived from Solanum nigrum induces apoptosis of human cholangiocarcinoma QBC939 cells. Oncol. Lett. 15, 6329–6335. https://doi.org/10.3892/ol.2018.8171.